NeuroImage xxx (2016) xxx–xxx

Contents lists available at ScienceDirect

NeuroImage

journal homepage: www.elsevier.com/locate/ynimg

Physiological processes non-linearly affect electrophysiological recordings during transcranial electric stimulation

Nima Noury [a,b,*], Joerg F. Hipp [a,c], Markus Siegel [a,*]

[a] Centre for Integrative Neuroscience & MEG Center, University of Tübingen, Germany
[b] IMPRS for Cognitive and Systems Neuroscience, Tübingen, Germany
[c] F. Hoffmann-La Roche, Pharma Research and Early Development, Basel, Switzerland

ARTICLE INFO

Article history:
Accepted 24 March 2016
Available online xxxx

Keywords:
Transcranial electric stimulation (tES)
Transcranial alternating current stimulation (tACS)
Transcranial direct current stimulation (tDCS)
EEG
MEG
Neural entrainment
Stimulation artifacts

ABSTRACT

Transcranial electric stimulation (tES) is a promising tool to non-invasively manipulate neuronal activity in the human brain. Several studies have shown behavioral effects of tES, but stimulation artifacts complicate the simultaneous investigation of neural activity with EEG or MEG. Here, we first show for EEG and MEG, that contrary to previous assumptions, artifacts do not simply reflect stimulation currents, but that heartbeat and respiration non-linearly modulate stimulation artifacts. These modulations occur irrespective of the stimulation frequency, i.e. during both transcranial alternating and direct current stimulations (tACS and tDCS). Second, we show that, although at first sight previously employed artifact rejection methods may seem to remove artifacts, data are still contaminated by non-linear stimulation artifacts. Because of their complex nature and dependence on the subjects' physiological state these artifacts are prone to be mistaken as neural entrainment. In sum, our results uncover non-linear tES artifacts, show that current techniques fail to fully remove them, and pave the way for new artifact rejection methods.

Introduction

Manipulative approaches are much needed in systems neuroscience. Take neuronal oscillations as an example. They are ubiquitous in the brain and have been implicated in various functions (Buzsáki and Draguhn, 2004; Fries, 2005; Jensen and Mazaheri, 2010; Siegel et al., 2012; Singer, 1999; Womelsdorf et al., 2014). However, supporting evidence, especially in humans, remains largely correlative and only few studies have addressed this causally (Helfrich et al., 2014; Marshall et al., 2006; Polanía et al., 2012; Romei et al., 2011, Romei et al., 2010; Voss et al., 2014). One strategy to causally assess potential roles of neural oscillations is to manipulate them and to simultaneously measure the effect on neural activity and behavior. This is technically challenging and well-defined experimental protocols as well as analysis pipelines have not been established yet.

Transcranial electric stimulation (tES) is a non-invasive brain stimulation technique, which provides the possibility to control stimulation strength, frequency and, to some extent, stimulation site (Dmochowski et al., 2011; Kanai et al., 2008; Schutter and Hortensius, 2010; Schwiedrzik, 2009). These features render tES and in particular one of its variants, transcranial alternating current stimulation (tACS), suitable for manipulating specific brain rhythms (Herrmann et al., 2013). During tACS, a sinusoidal electrical current at a specific frequency is applied to the subject through electrodes placed on the scalp. The potential of electrical stimulation to manipulate neuronal oscillations has been shown in animal models (Fröhlich and McCormick, 2010; Ozen et al., 2010). However, in humans, tACS has largely been limited to investigating effects on behavior and on neurophysiological aftereffects (Brittain et al., 2013; Herrmann et al., 2013; Marshall et al., 2011, Marshall et al., 2006; Polanía et al., 2012; Zaehle et al., 2010). A key reason for the limited number of studies directly investigating effects on neural activity during stimulation is the massive electrophysiological artifact induced by the stimulation. These artifacts are particularly problematic when attempting to investigate effects on neuronal activity within the same frequency range as the stimulation frequency (Zaehle et al., 2010).

Recently, different approaches have been proposed to remove tES artifacts from EEG and MEG for studying neuronal activity during stimulation (Helfrich et al., 2014; Neuling et al., 2015; Soekadar et al., 2013; Voss et al., 2014). Based on the assumption of linear stimulation artifacts, these methods follow approaches like template subtraction, component analysis, beamforming or temporal filtering. However, a thorough characterization of stimulation artifacts, which is needed for assessing artifact cleaning procedures, is missing. Here we provide this characterization.

* Corresponding authors at: Centre for Integrative Neuroscience, University of Tübingen, Otfried-Müller-Str. 25, 72076 Tübingen, Germany.
E-mail addresses: nima.noury@cin.uni-tuebingen.de (N. Noury), markus.siegel@uni-tuebingen.de (M. Siegel).

http://dx.doi.org/10.1016/j.neuroimage.2016.03.065
1053-8119/

Materials and methods

Methods outline

We measured EEG and MEG during several different tES conditions. First, we tested if a pure sinusoidal model can explain tES artifacts. Next, we investigated in the time and frequency domain whether heartbeat and respiration modulate tES artifacts. Finally, we used temporal and spectral features of tES artifacts to track them through different stages of available artifact rejection pipelines. The rationale behind each analysis is explained in the Results section.

Participants and experimental protocol

All experiments were conducted in 5 healthy male participants. All subjects gave written informed consent before participating. All experiments were conducted in accordance with the Declaration of Helsinki and approved by the local ethics committee. The main tACS experiment with small stimulation electrodes was conducted in 4 subjects that each participated in 6 experimental runs. Each run consisted of the following sequential conditions: sham, tACSa, tACSb, sham, tACSb, and tACSa. Each condition lasted 66 s. For each run, 11 Hz tACS and 62 Hz tACS were randomly assigned to tACSa and tACSb conditions to avoid any potential sequence effects. During the first 5 runs, subjects fixated a central fixation spot at the center of a blank monitor (60 Hz refresh rate). In the last run subjects kept their eyes closed. Before start of the experiment, subjects were habituated to transcranial electric stimulation. In one of the four subjects, we performed a control experiment with large rubber electrodes. In this control experiment runs 3 and 6 were measured with eyes closed. We performed two more control experiments on a fifth subject with the same electrode layout as in the main tACS experiment. In both experiments, the subject fixated a central fixation spot. In the first control experiment, we checked for the potential influence of the EEG ground electrode placement on the stimulation artifact during 62 Hz tACS. We recorded 10 min of EEG with ground on the right forearm and 10 min with ground on the forehead (Fpz of 10–10 system). In the second control experiment, we recorded MEG and EEG during cathodal tDCS, anodal tDCS and sham conditions (10 min per condition). Cathodal and anodal are defined based on the polarity of the parietal stimulation electrode.

Transcranial electric stimulation

Stimulation current was applied with an IZ2h stimulator (Tucker Davis Technologies Inc.). Stimulation amplitude was 0.5 mA (i.e., 1 mA peak-to-peak for tACS). Stimulation did not induce flicker percepts. For the main experiment, stimulation was applied through two standard Ag/AgCl EEG electrodes over right occipital and right parietal areas (electrodes O10 and CP4 of the 10–10 electrode system). For the control experiment with large electrodes, 35 cm^2 MR-compatible rubber electrodes (neuroConn GmbH) were placed over occipital and frontal lobes underneath the EEG cap. For all experiments, stimulation electrodes were attached using Ten20 conductive paste (Weaver and Company) and their impedance was kept below 2.5 kΩ. To minimize magnetic artifacts produced by the stimulation current, we carefully twisted all stimulation cables.

Data acquisition and preprocessing

We simultaneously recorded 72-channel EEG (NeurOne system, Mega Electronics Ltd) and 272-channel MEG (Omega 2000, CTF Systems) throughout all experiments at 10,000 Hz and 2343.8 Hz sampling rate, respectively. EEG electrodes were positioned based on the 10–10 electrode system using an EEG cap (EC80, EASYCAP). All signals were in the dynamic range of recording systems and no clipping was observed for either EEG or MEG signals. Due to the interference between stimulation currents and electrical currents of the head-positioning circuits of the MEG system, we could not monitor head movement continuously during the experiment. Instead we measured head positions at the beginning and at the end of each run.

EEG electrodes were attached using Abratyl 2000 conductive gel and impedances were kept below 2.5 kΩ for most electrodes. We referenced EEG electrodes to FCz and, except for one control experiment, positioned a ground electrode on the right forearm. EEG signals were re-referenced to average reference offline. Along with EEG and MEG, we recorded the injected current, the ECG and respiratory movements using bipolar channels of the EEG system. The injected current was indirectly measured by recording the voltage drop across a 200 Ω resistor positioned in series to the head. The ECG was recorded through 2 electrodes placed below the right clavicle and below the left pectoral muscle. Respiration was continuously recorded with a piezo respiratory belt transducer (Vermed-Medizintechnik).

Sinusoidal model subtraction

To remove an optimal sinusoidal model from artifactual signals, we fitted the amplitude, frequency and phase of a sinusoid to the MEG and EEG data and subtracted it from the data. For this, it is important to estimate the stimulation frequency with μHz accuracy. This is because, if the internal clocks of the stimulation and recording system are not synchronized, as in the present case, even small errors of the estimated stimulation frequency lead to strong residual artifacts around the main peak. To this end, we first chose 20 MEG channels with strongest tACS artifacts and split their data into 33 s long segments on which we fitted amplitude, frequency and phase of a sinusoidal model separately for each channel. We estimated the stimulation frequency as the median across all segments and channels (standard deviation of 8.50 and 4.85 μHz, for 11 Hz and 62 Hz tACS, respectively). Next, we defined a new sinusoidal model fixing its frequency at the estimated stimulation frequency. We then separately fitted amplitude and phase of this new model to each segment and channel and removed it from the data.

We followed a similar strategy for EEG. As we also recorded the injected current with the EEG system, this allowed for estimating the stimulation frequency based on the injected current. This is more accurate than estimation based on the EEG signal, because the injected current does not include any brain signals. As for the MEG, we split the injected current into 33 s long segments and estimated the stimulation frequency for each piece. We estimated the stimulation frequency as the median across all segments (standard deviation of 0.10 and 0.66 μHz, for 11 Hz and 62 Hz tACS, respectively).

Spectral analyses

To estimate the power spectral density (PSD) in tACS experiments, we first split the data into either 4 s or 33 s long segments, according to the desired spectral resolution. Then, we applied a Hanning window to each segment and computed its Fourier transform. Finally, we calculated the average power across all segments and scaled the results to PSD (μV^2/Hz and fT^2/Hz for EEG and MEG, respectively). For the case of tDCS and to reveal the spectral structure of artifacts in face of strong low frequency activity of EEG and MEG, we estimated spectra with higher resolution. We split the data into 120 s segments, estimated the Thomson's multitaper PSD of each segment (Slepian tapers with 0.05 Hz bandwidth, NW = 6) and calculated the average power across all segments.

Heartbeat and respiration frequencies

For each subject, heartbeat and respiration rates were defined as the inverse of the median of the temporal intervals between successive ECG R-peaks and respiration ends, respectively.

Please cite this article as: Noury, N., et al., Physiological processes non-linearly affect electrophysiological recordings during transcranial electric stimulation, NeuroImage (2016), http://dx.doi.org/10.1016/j.neuroimage.2016.03.065

Temporal analyses

For all analyses of tACS artifact envelopes, we first band-pass filtered the recorded signals using a 6th-order zero-phase Butterworth filter centered at the stimulation frequency of interest with a pass-band of ±5 Hz. For all comparisons between sham and tACS conditions, we filtered the sham data with the same filter that we applied to the corresponding tACS data. After band-pass filtering, we down-sampled EEG and MEG signals to 1000 Hz and 781.25 Hz, respectively, and applied the Hilbert transform to obtain signal envelopes. To investigate heartbeat and respiration locked modulations, we extracted 4 s or 8 s long envelope segments centered on all ECG R-peaks or inspiration ends, respectively. We subtracted the temporal mean from each segment and tested a significant modulation at each time point using permutation statistics: We compared the average envelope across all segments against the distribution of average envelopes from 1000 random placements of segments on the data. We converted the resulting p-values to z-scores for displaying modulation envelopes. We Bonferroni-corrected p-values for the number of time points to assess the significance of modulation for each channel.

For testing the effect of heartbeat and respiration on the tDCS artifact, we band-pass filtered the recorded signals using a 6th-order zero-phase Butterworth filter between 0.05 and 5 Hz, extracted 4 s long heartbeat-locked and 8 s long respiration-locked segments, removed the mean of each segment, and applied the same permutation statistics as for tACS.

We performed an adapted PCA on the average heartbeat and respiration locked envelopes to test the temporal stability of spatial artifact patterns. For each sensor, we calculated the average of all envelope segments without removing their mean. These average envelopes contain the amplitude of the constant sinusoidal artifacts (the temporal mean of the envelopes) together with their heartbeat locked modulation. We derived the temporal mean of the envelopes of all channels as the first PC. We then removed this first PC from the average envelopes and applied PCA on the zero-mean envelopes to derive the remaining PCs.

AM-transformation of modulation kernel

For each channel and each subject, we refer to the mean-removed average of all heartbeat-locked modulations as the heartbeat kernel. To calculate the AM-transformed heartbeat kernel (Fig. 5), we applied the AM model and simply multiplied the kernel with a 62 Hz sinusoidal wave.

Template subtraction and PCA based artifact removal

We applied the procedure used by Helfrich et al. (2014) on the EEG data recorded during 11 Hz tACS with small stimulation electrodes of one subject. We first band-pass filtered the data between 1 Hz and 35 Hz using a 4th-order zero-phase Butterworth filter and up-sampled the data to 30 kHz. Next, we split one channel's signal into 3 s long segments and adjusted the temporal position of each segment to maximize its correlation with the first segment. We segmented all remaining channels according to these adjusted alignments. Next, for each segment and channel, we calculated an artifact template by averaging the ten adjacent segments. To construct the template-subtracted signal, each segments' template was regressed out from the corresponding segment.

In a second step, we applied PCA on the template-subtracted data. For investigating heartbeat-related modulations of the resultant PCs, we first extracted heartbeat-locked segments from 0.7 s prior to 1 s after ECG R-peaks. As the method applied by Helfrich et al. (2014) cuts the data into 3-s segments, we restricted the analysis on heartbeats for which the entire 1.7 s interval fell in one segment (about one third of heartbeats). For each heartbeat-locked segment, we computed the envelope of 11 Hz power using a sliding window Fourier-analysis (0.5 s Hanning window, 0.1 s step size). Because the first template-subtraction step destroyed the consistent heartbeat-locked envelope modulation, it became more difficult to track the non-linear artifact during the second step (PCA). Notably, the difficulty to track the artifact does not imply that it is gone. To overcome this problem, we devised a 3-step procedure. PC1 strongly captured the stimulation artifact (Fig. 8c): The topography reflected the position of stimulation electrodes, the power spectrum showed symmetric peaks around the stimulation frequency, and 11 Hz power was significantly modulated by each heartbeat ($P < 0.05$; permutation test). We used these features of PC1, to identify additional artifactual PCs. First, we tested which PCs show heartbeat-locked modulations of 11 Hz power significantly correlated to the heartbeat-locked modulation of PC1. 9 PCs showed this artifactual feature, even though their topographies seemed physiological ($P < 0.05$ uncorrected). Second, we employed a similar analysis to also account for non-linear artifacts not locked to heartbeats. We tested which PCs showed a significant correlation of modulations of 11 Hz power to modulations of PC1 across all 3-s segments. We found 8 PCs out of the remaining 62 PCs that showed significantly correlated modulations ($P < 0.05$ uncorrected). Third, as a simple spectral heuristic for additional potentially artifactual PCs, we checked which PCs showed symmetric peaks around the stimulation frequency in their spectrums. We found that among 54 remaining PCs, 18 showed this symmetricity of their power spectrum.

Beamforming

We applied adaptive linear spatial filtering (beamforming) (Van Veen et al., 1997) to the MEG data of the final two runs of tACS stimulation with small stimulation electrodes, which includes one run with eyes open and one run with eyes closed. We first band-passed the data using a 6th-order zero-phase Butterworth high-pass filter at 2 Hz and a low-pass filter at 90 Hz. Afterwards we notch filtered the line noise by means of a 6th-order zero-phase Butterworth band-stop filter from 49.8 Hz to 50.2 Hz band. We down sampled the data to 585.94 Hz and calculated the covariance matrix based on the concatenated data of the 11 Hz tACS and sham conditions of both runs. For tACS recordings, the high signal power caused by the stimulation artifact makes it difficult to determine the cutoff between brain signals and sensor noise. Thus, we set the regularization factor (λ), which is an estimate of measurement noise, based on sham recordings only. To this end, we applied PCA on the covariance matrix of sham recordings, and set the regularization factor equal to Eigenvalue of PC at which the cumulative explained variance reached 99% of the total variance. Finally, based on the covariance matrix and regularization factor, for each source location, we calculated three orthogonal filters (one for each spatial dimension) and linearly combined them to a single filter in the direction of maximum variance.

Source locations and physical forward model

We performed the beamforming analysis on a regular three-dimensional grid that covered the whole brain with 1-cm spacing in MNI space (2982 source locations). We nonlinearly transformed source locations into individual head space using the participants' individual T1-weighted structural MRI. The MEG sensors were aligned to the head geometry on the basis of three fiducial points (nasion, left ear, right ear) that were registered before and after the MEG acquisition by three head localization coils. To derive the physical relation between sources and sensors (leadfield), we employed a single-shell head model (Nolte, 2003).

Source-space analysis

We computed the ratio of source-level alpha power (8–14 Hz) between eyes open and eyes closed conditions, to test if beamforming during tACS was able to reveal physiological activity. To this end, we band-pass filtered the source-level time-courses from 8 to 14 Hz using

Please cite this article as: Noury, N., et al., Physiological processes non-linearly affect electrophysiological recordings during transcranial electric stimulation, NeuroImage (2016), http://dx.doi.org/10.1016/j.neuroimage.2016.03.065

a 4^{th} order zero-phase Butterworth filter and divided the variance of eyes closed time-courses by the variance of eyes open time-courses. To assess the significance of alpha-power modulation we compare the log power of 2 s segments between eyes open and eyes closed conditions (120 segments each) using t-statistics. To test if source-level activity was contaminated by the non-linear stimulation artifact, we estimated the power spectrum at each source position with 0.05 Hz resolution (20 s segments, Hanning window). We then computed the linear correlation (Pearson's r) between the brain-wide distribution of 11 Hz power and the distribution of power at all other frequencies. We tested if this correlation peaked specifically at the stimulation frequency ± the heart rate.

Analysis software

All data analyses were performed in Matlab (MathWorks) using custom scripts and the open source toolbox Fieldtrip (Oostenveld et al., 2011).

Results

tACS artifacts in EEG and MEG

We recorded EEG and MEG during 11 Hz tACS, 62 Hz tACS, and sham stimulation in 4 subjects. Stimulation currents were injected through two Ag/AgCl electrodes with 1 mA peak-to-peak strength (Fig. 1a). EEG was recorded through the 72 remaining electrodes of the 10–10 electrode system, along with 272 MEG channels. Throughout the experiment, we also recorded the electrocardiogram (ECG) and respiration of subjects. For both, EEG and MEG, during stimulation, signals showed strong artifacts at tACS frequencies (Fig. 1b–g). These stimulation artifacts were observed at almost all electrodes with a spatial distribution that reflected the location of stimulation electrodes. At electrodes near the stimulation site, artifacts were more than 1000 times bigger than neural signals. In the frequency domain, artifacts manifested as a main peak at the stimulation frequency together with its harmonics. This reflected the spectral peaks of the stimulation current (Supplementary Figure 1a, b).

Nonlinear effect of heartbeat and respiration

To characterize the tACS artifact in more detail, we first evaluated the performance of the stimulation system and tested if, as intended, the main peak of the stimulation current resembled a pure sinusoid. This is critical, because any imperfection of the stimulation current would be reflected in the stimulation artifact. Subtracting an optimum sinusoidal model from the injected current almost perfectly removed the main peak (more than 100 dB suppression; Fig. 2a, b; Materials and methods). Thus, the main stimulation peak of the injected current well resembled a pure sinusoid.

Next, we characterized stimulation artifacts on EEG and MEG. A key question about the nature of these artifacts is if they reflect a simple sinusoid as the injected current, or if they show more complex characteristics. To test this, we performed the same analysis as for the stimulation current and removed a sinusoidal artifact model from the EEG and MEG during tACS (Fig. 2c–f). This indeed removed the main stimulation peak for 11 Hz and 62 Hz tACS. However, high-resolution spectra revealed that, in contrast to the stimulation current, many EEG and MEG channels showed prominent side peaks up to several Hertz around the stimulation frequency. These side peaks remained after removing the sinusoidal model (see Supplementary Figure 2 for a larger frequency range). Thus, stimulation effects on EEG and MEG were not purely sinusoidal as the stimulation current. Does this reflect neural entrainment?

Notably, side peaks in EEG and MEG were symmetric around the stimulation frequency and very similar for 11 Hz and 62 Hz tACS. These characteristics suggested that side peaks reflected a non-linear process underlying artifact generation, rather than neural entrainment. Symmetric side-peaks around a central frequency are reminiscent of the amplitude modulation (AM) technique that is used in electronic communication. In this technique, the amplitude of a high-frequency sinusoidal carrier is modulated by a low frequency signal. This results in a

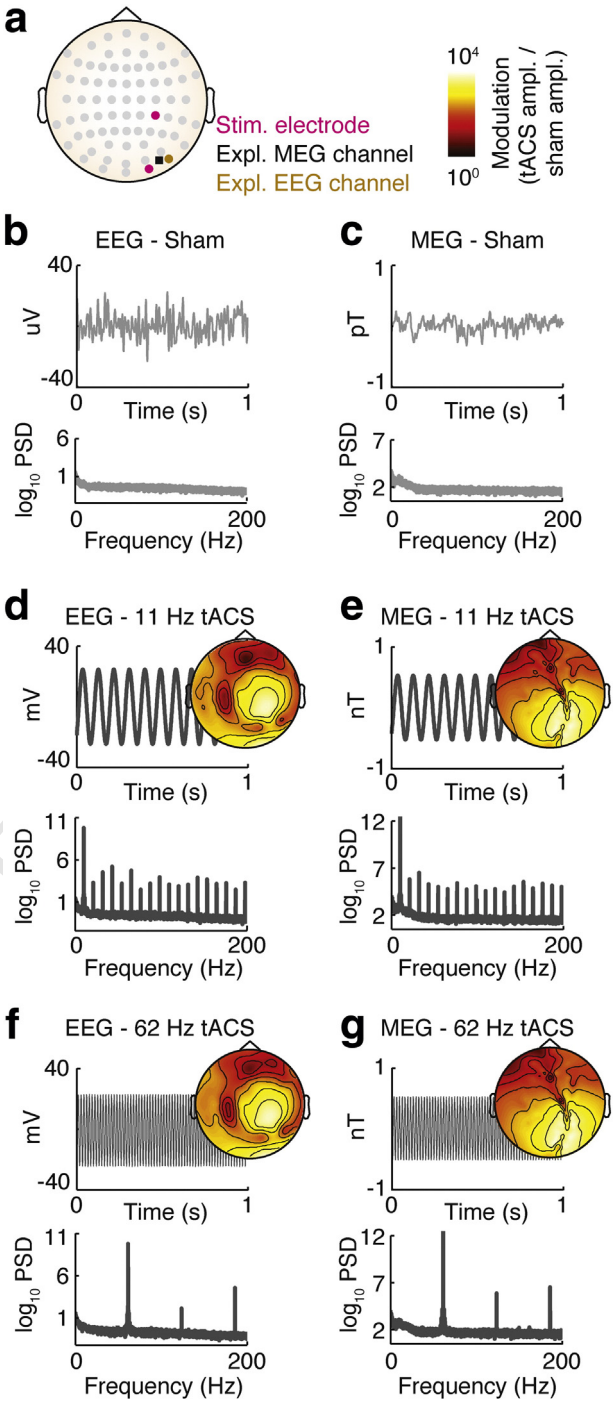

Fig. 1. Simultaneous tACS, EEG, and MEG. (*a*) EEG and tACS were performed with 74 Ag/AgCl electrodes placed according to the 10–10 system. Purple circles indicate the position of the stimulation electrodes. The brown circle and black square indicate the position of channels used for demonstrating EEG (PO10) and MEG (MRT57) results, respectively. (*b*) Typical EEG signal and average EEG power spectral density during sham. (*c*) Typical MEG signal and average MEG power spectral density during sham. (*d*) EEG and (*e*) MEG signals and spectra during 11 Hz tACS. (*f*) EEG and (*g*) MEG signals and spectra during 62 Hz tACS. Topographies show the strength of artifacts, quantified as decadic logarithm of the standard deviation of signals during tACS divided by standard deviation of signals during sham. This figure shows data from subject S1, during one experimental run with eyes open.

Please cite this article as: Noury, N., et al., Physiological processes non-linearly affect electrophysiological recordings during transcranial electric stimulation, NeuroImage (2016), http://dx.doi.org/10.1016/j.neuroimage.2016.03.065

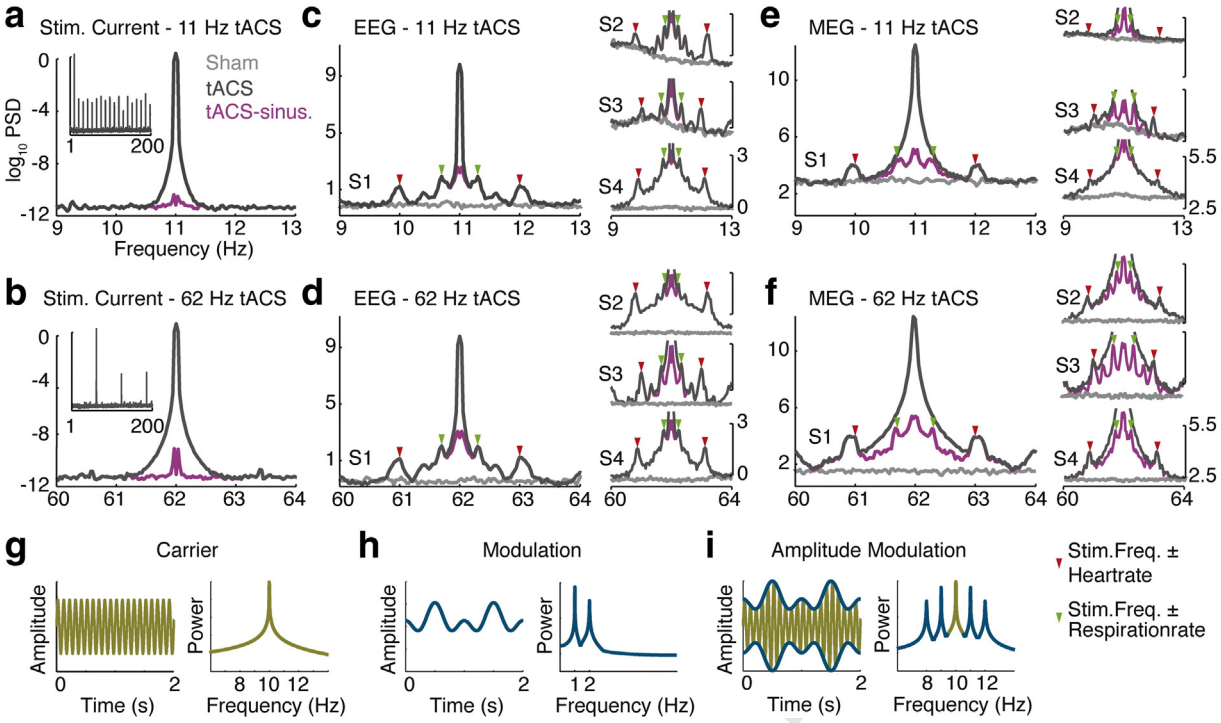

Fig. 2. Stimulation artifacts in the frequency domain. (*a*, *b*) Power spectral density of the stimulation current around the stimulation frequency for 11 Hz and 62 Hz tACS. Subtracting a sinusoidal model from the stimulation current (magenta) removed almost all power. (*c*) EEG power spectral density around the stimulation frequency during sham and 11 Hz tACS, with and without removal of a sinusoidal artifact model. The large spectrum shows data from subject S1. Smaller spectra show all other subjects. Red and green arrows mark the stimulation frequency ± individual average heartbeat and respiration frequencies, respectively. (*d*) EEG spectra for 62 Hz tACS. (*e*) MEG spectra for 11 Hz tACS. (*f*) MEG spectra for 62 Hz tACS. Subtracting the sinusoidal artifact model reveals the symmetric spectral peaks. See Supplementary Figure 2 for a wider frequency range. EEG and MEG data show channels PO10 and MRT57, respectively. (*g*, *h*, and *i*) Schematic illustration of amplitude modulation (AM) in time and frequency domains. The amplitude of a carrier signal (*g*) is modulated by a slower modulation signal (*h*), which results in the amplitude-modulated signal (*i*). In the frequency domain, this corresponds convolution of modulation and carrier spectra, which results in a symmetric spectrum, where the spectrum of the modulation signal is symmetric around the peak of the carrier frequency.

spectrum with symmetric side-peaks, which reflect the low-frequency signals' spectrum around the carrier frequency peak (Fig. 2g–i). The fact that we found side peaks positioned symmetrically around the stimulation frequency (Fig. 2) suggested that AM modulation may be involved in the non-linear stimulation artifact. Which processes may modulate the stimulation artifact? We hypothesized that this may be the subjects' heartbeat and respiration. If that was true, spectra should show side peaks at the stimulation frequency ± individual heartbeat and respiration frequencies. Indeed, for each subject, we found four side peaks at exactly the predicted frequencies (Fig. 2c–f).

To directly test our hypothesis in the time domain, we performed a time-locked analysis in which we averaged the M/EEG signals' envelope at the stimulation frequency temporally aligned on heartbeats (Fig. 3a–d). Indeed, in all subjects we consistently found that the heartbeat strongly modulated the main stimulation artifact. This modulation happened for both EEG and MEG, and irrespective of the stimulation frequency. Almost all M/EEG channels showed a significant modulation by heartbeat ($p < 0.05$ corrected, permutation test) with strongest effects close to the stimulation site. Effects were clearer for 62 Hz stimulation frequency likely reflecting weaker electrophysiological signals at that frequency (see also Supplementary Figure 2). Importantly, for many channels the strength of non-linear modulation was even bigger than strength of neural signals recorded during the sham condition (Fig. 3 topographies).

Control analyses

Any change in the injected current influences the stimulation artifact. Thus, we performed a control analysis and tested if the injected current showed heartbeat-locked modulations. We did not find any side-peaks around the stimulation frequency and no heartbeat-locked modulations of the injected current (Fig. 2a, b and Supplementary Figures 1c, d). This rules out that the heartbeat-locked modulations of artifacts were driven by variations of the injected current.

In another control analysis, we investigated if the non-linear stimulation artifact reflected the well-known electro- and magnetocardiogram (E/MCG; Supplementary Figure 3). To this end, we removed the average E/MCG around each heartbeat. This had no effect on the heartbeat-locked envelope modulation during tACS. In sum, we concluded that the non-linear stimulation artifact neither was driven by modulation of the stimulation current nor merely reflected the E/MCG.

Spatial stability of heartbeat-locked non-linear artifact

We next investigated if the heartbeat-locked non-linear artifact had a constant spatial pattern over time similar to the spatial pattern of the main stimulation peak. This is particularly important for potential artifact cleaning algorithms that employ linear decomposition or filtering, such as e.g. PCA, ICA or beamforming. To this end, we employed an adapted PCA and tested if the stimulation artifact's envelope was captured in one component (Fig. 3e–f; see Materials and methods). The first principal component captured the average stimulation artifact together with part of its modulation over time. However, in addition to the first components, 6 additional components for EEG and 3 additional components for MEG also showed clear rhythmic modulations (Fig. 3e–f). Accordingly, the relation between rhythmically modulated components was not constant over time. Thus, the spatial pattern of the stimulation artifact was not constant over time, but was modulated by heartbeats, for both EEG and MEG.

Respiration-locked modulation

We repeated the time-locked analysis using the respiration signal (Fig. 4a–d). Irrespective of stimulation frequency, artifact envelopes of

Please cite this article as: Noury, N., et al., Physiological processes non-linearly affect electrophysiological recordings during transcranial electric stimulation, NeuroImage (2016), http://dx.doi.org/10.1016/j.neuroimage.2016.03.065

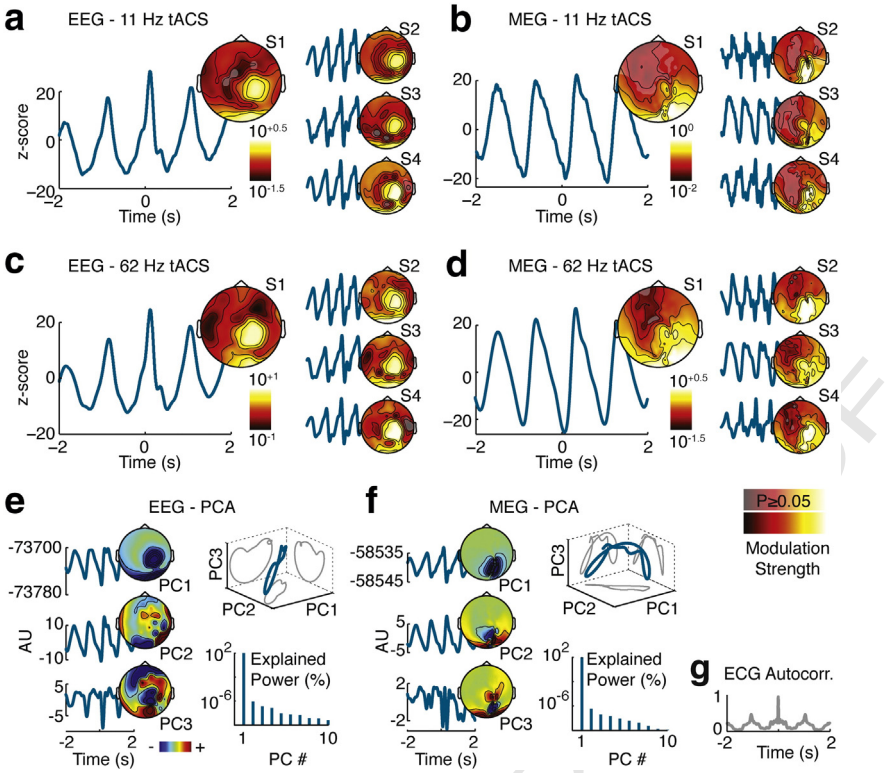

Fig. 3. Heartbeat locked artifacts. (*a*) Time-courses depict the modulation of the EEG envelope around the time of heartbeats during 11 Hz tACS quantified as the statistical z-score against a null-hypothesis of no modulation. The topography shows the strength of modulation relative to the neural signal of interest quantified as the decadic logarithm of the standard deviation of heartbeat-locked modulation divided by standard deviation of the sham signal at the stimulation frequency (non-significant modulations are masked at P = 0.05 corrected). The large panel shows data from subject S1. Smaller panels show all other subjects. (*b*) Heartbeat locked modulation of MEG envelope during 11 Hz tACS. (*c*) Heartbeat locked modulation of EEG envelope during 62 Hz tACS. (*d*) Heartbeat locked modulation of MEG envelope during 62 Hz tACS. EEG and MEG data show channels PO10 and MRT57, respectively. (*e*) PCA of average heartbeat-locked EEG envelope modulations during 62 Hz tACS. Shown are the first 3 PCs in the time domain together with their sensor topographies (eigenvectors). PCs are sorted by explained power as indicated in the lower right panel. The top right panel shows the average heartbeat-locked modulation time-course projected on the first three PCs. (*f*) PCA of average heartbeat-locked MEG envelope modulations during 62 Hz tACS. (*g*) Autocorrelation of the ECG.

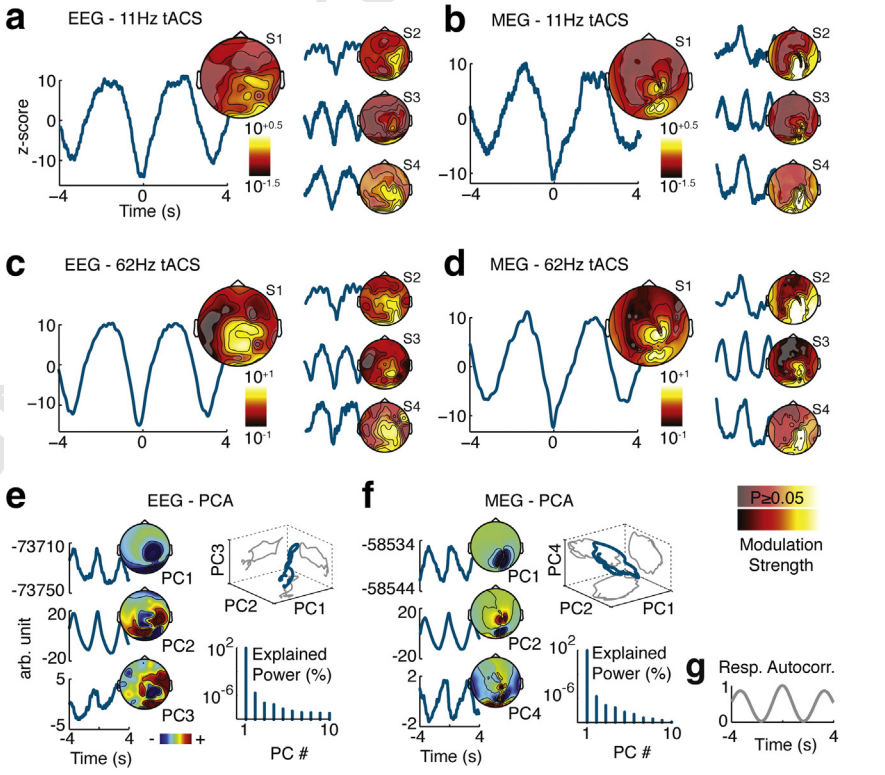

Fig. 4. Respiration locked artifacts. Modulation of (*a*) EEG and (*b*) MEG envelope by respiration during 11 Hz tACS. Modulation of (*c*) EEG and (*d*) MEG envelope by respiration during 62 Hz tACS. PCA of average heartbeat-locked (*e*) EEG and (*f*) MEG envelope modulations during 62 Hz tACS. (*g*) Autocorrelation of the respiration signal. All other conventions as in Fig. 3.

Please cite this article as: Noury, N., et al., Physiological processes non-linearly affect electrophysiological recordings during transcranial electric stimulation, NeuroImage (2016), http://dx.doi.org/10.1016/j.neuroimage.2016.03.065

most EEG and MEG channels were strongly modulated by respiration ($p < 0.05$ corrected, permutation test). Similar to heartbeat-locked modulations, for many channels, respiration-related modulations were stronger than neural activity and were easier observable for 62 Hz than for 11 Hz tACS. e performed a control analysis of the injected current and ruled out any influence of the injected current on the observed respiration-locked artifact (Supplementary Figures 1e–f). Again, we performed an adapted PCA on the average respiration locked envelopes, to check if respiration-locked modulations showed a stable spatial pattern over time (Fig. 4e–f). Similar as for the heartbeat-locked effect, we found that PCA did not capture the artifact in one principal component. Thus, we concluded that, alike heartbeats, respiration non-linearly modulated the strength and spatial pattern of the stimulation artifact over time.

Ground electrode

We checked whether the stimulation artifacts observed in EEG may be related to the position of the EEG ground electrode. Thus, in one subjects we recorded two sessions of EEG signals during 62 Hz tACS with the ground electrode positioned on either the forearm or forehead. We observed very similar stimulation artifacts for both ground positions (Supplementary Figure 4). Thus, we concluded that heartbeat-locked and respiration-locked stimulation artifacts are not related to the position of the ground electrode.

Bandwidth of non-linear stimulation artifact

We next assessed the spectral extent of the non-linear stimulation artifact (Fig. 5). Heartbeat and respiration modulations are not purely sinusoidal (Figs. 3 and 4) and may thus affect M/EEG signals during tACS beyond the side peaks directly related to heart and respiration rate. Because heart rate is high compared to respiration rate, in particular harmonics of heart rate may contaminate electrophysiological signals in a wide frequency band. To investigate this, similar to the AM model, we multiplied the average heartbeat-locked envelope artifact, which in the following we term the heartbeat kernel, with a sinusoid at the stimulation frequency and compared the resultant power spectrum to the measured spectrum. Indeed, in all subjects, all peaks of the transformed heartbeat kernels well matched the symmetric peaks of M/EEG spectra during tACS. Importantly, these peaks reached ± 10 Hz beyond the stimulation frequency. Furthermore, because subjects showed different modulation patterns, the artifact bandwidth and spectral pattern was unique for each subject. We concluded that the non-linear stimulation artifact affected M/EEG signals during tACS up to 10 Hz around the stimulation frequency.

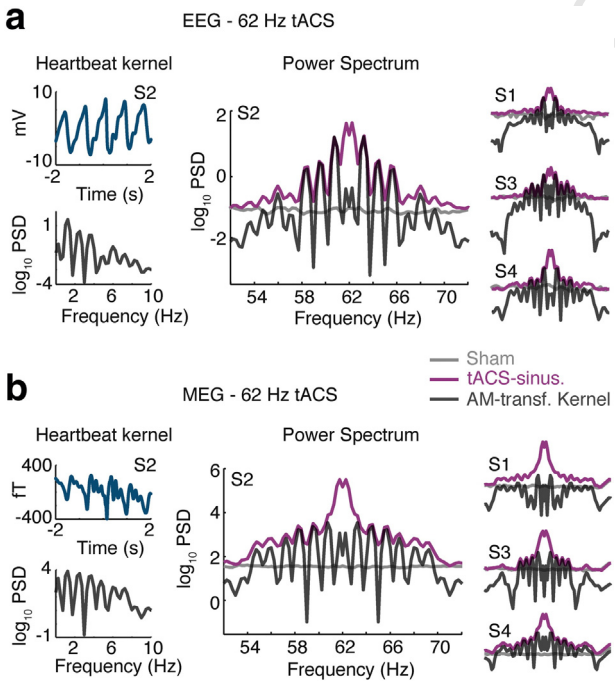

Fig. 5. AM transformation of heartbeat kernel. (*a*) Left panels depict the average heartbeat-locked EEG envelope modulation (heartbeat kernel) in time (top) and frequency (bottom) domains for subject S2 (channel PO10). The central panel shows EEG power spectral density for 62 Hz tACS, sham, and the AM-transformed heartbeat kernel. Smaller panels on the right show all other subjects. For tACS spectra, the main stimulation artifact was removed by subtracting a sinusoidal artifact model (*b*) AM transformation of heartbeat kernel for MEG during 62 Hz tACS. EEG and MEG data show channels PO10 and MRT57, respectively.

Electrode size

In contrast to the small stimulation electrodes used here, many tACS studies use big rubber electrodes for stimulation. Thus, we repeated the experiments with big rubber electrodes in one subject, to test if our results may depend on the size of stimulation electrodes (Fig. 6). We found the same results for big rubber electrodes indicating that the observed artifacts are not related to electrode size.

In sum, our results demonstrate non-linear tACS artifacts related to physiological processes (heartbeat, respiration) that have a variable topography, are on the order of concurrent electrophysiological signals of interest, and are consistently found in all tested subjects. These artifacts pose a substantial problem for assessing neuronal activity during tACS.

tDCS artifact

The observed heartbeat-locked and respiration-locked tACS artifacts occur irrespective of the stimulation frequency. Thus, we hypothesized that the same artifacts also interfere with EEG and MEG during transcranial direct current stimulation (tDCS), which can be interpreted as tACS at 0 Hz. To test this, we performed a control experiment, in which we recorded EEG and MEG during cathodal and anodal tDCS. Indeed, the recorded EEG and MEG signals showed heartbeat and respiration related artifacts similar to tACS artifacts in both, frequency and time domains (Fig. 7). High-resolution spectra of EEG and MEG signals showed clear peaks at the individual's heart rate and its harmonic during both cathodal and anodal tDCS (filled and open red triangles in Fig. 7). Concerning respiration, strong neural signals below 1 Hz masked potential peaks at the individual's respiration rate (filled green triangles in Fig. 7), but peaks at the first harmonic of the respiration rate were clearly visible in the power spectrum (open green triangles in Fig. 7). Next, we applied heartbeat-locked and respiration-locked analyses in the time domain. Similar to tACS, recordings during tDCS showed strong rhythmic modulations locked to heartbeat and respiration (Fig. 7). The opposite polarity of these artifacts for cathodal and anodal stimulation as well as the artifact topography show that these modulations do not merely reflect the well-known electro- and magnetocardiogram (E/MCG) or respiration artifacts that are also observable during the sham condition. In sum, we concluded that EEG and MEG recordings during tDCS show artifacts similar to tACS artifacts.

Available artifact rejection methods

Recently, different approaches have been proposed to clean EEG and MEG signals from tES artifacts (Helfrich et al., 2014; Neuling et al., 2015; Soekadar et al., 2013; Voss et al., 2014). As our above findings provide new insights into the extent and characteristics of stimulation artifacts, we tested if existing methods account for them (Fig. 8; see also Materials and methods).

A recent combined EEG and tACS study (Helfrich et al., 2014) adopted a method used in simultaneous EEG-fMRI studies (Niazy et al., 2005) for cleaning of tACS artifacts: First, an adaptive artifact

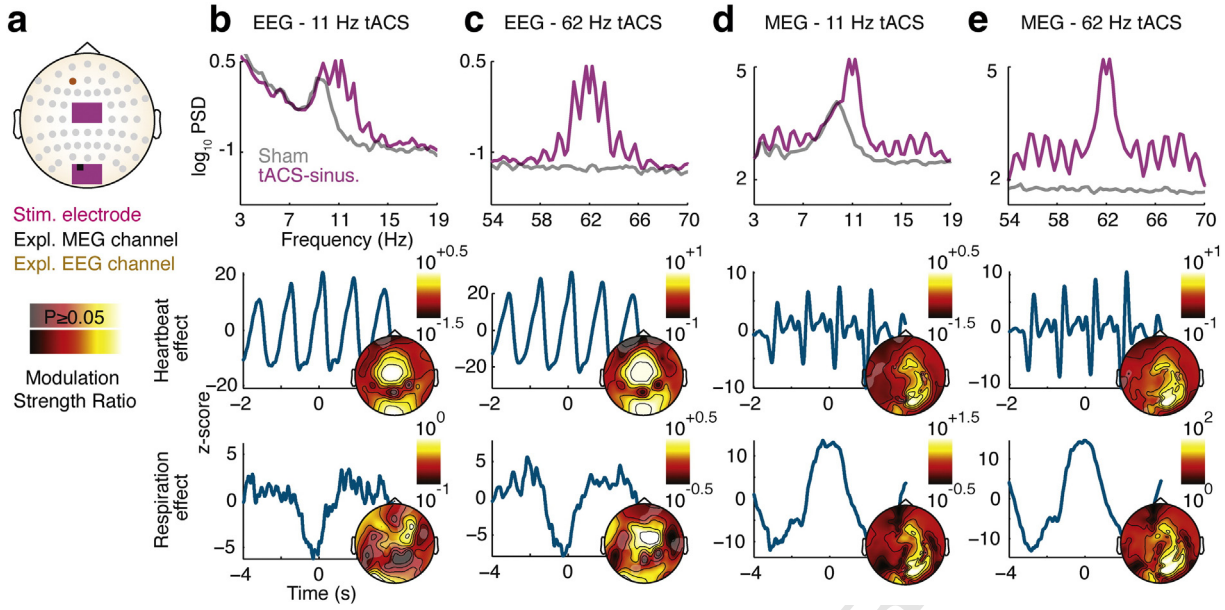

Fig. 6. tACS artifacts for large stimulation electrodes. (*a*) Two large rubber stimulation electrodes were positioned between 62 EEG electrodes placed according to the 10–10 system. The brown circle and black square indicate the position of channels used for demonstrating EEG (AF3) and MEG (MLO31) results, respectively. (*b*) The top panel shows the EEG power spectral density around the stimulation frequency during 11 Hz tACS and sham. The middle and bottom panels show heartbeat- and respiration-locked modulations of EEG envelope, respectively. Topographies show the strength of modulation relative to the neural signal of interest quantified as the decadic logarithm of the standard deviation of heartbeat-locked modulation divided by standard deviation of the sham signal at the stimulation frequency (non-significant modulations are masked at P = 0.05 corrected). (*c*) EEG artifacts for 62 Hz tACS. (*d*) MEG artifacts for 11 Hz tACS. (*e*) MEG artifacts for 62 Hz tACS.

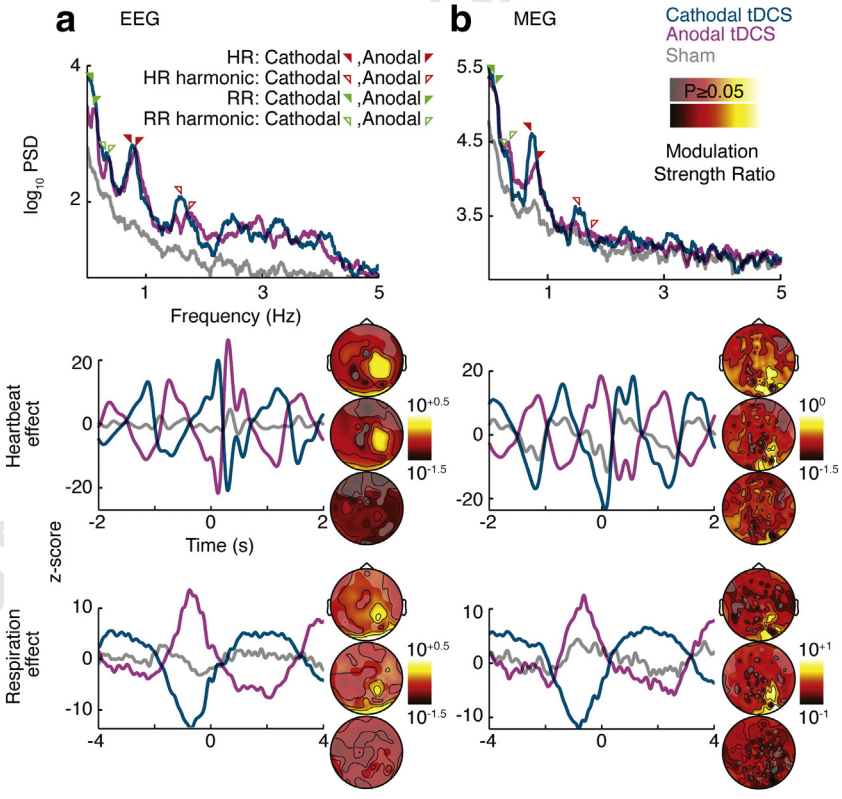

Fig. 7. tDCS artifacts. (*a*) Top panel shows the power spectral density of EEG signals during cathodal (blue) and anodal (pink) tDCS compared to sham (gray). Power spectra show peaks at heart rate (HR) and respiration rate (RR) related frequencies. Harmonic of each rhythm refers to twice its rate. Middle and bottom panels depict z-score of heartbeat-locked and respiration-locked modulations of EEG during cathodal and anodal tDCS. Polarity of modulations depends on stimulation polarity. The three topographies in each panel show the strength of the artifact for cathodal (top), anodal (middle) and sham (bottom) recordings. Artifact strength is quantified as the decadic logarithm of the standard deviation of heartbeat or respiration-locked modulations divided by standard deviation of the sham signal (non-significant modulations are masked at P = 0.05 corrected). (*b*) Heartbeat and respiration artifacts in MEG signals recorded during tDCS. All conventions as in (*a*). MEG artifacts during sham might be enhanced due to the stimulation and EEG setup. EEG and MEG data show channels PO10 and MZO2, respectively.

Please cite this article as: Noury, N., et al., Physiological processes non-linearly affect electrophysiological recordings during transcranial electric stimulation, NeuroImage (2016), http://dx.doi.org/10.1016/j.neuroimage.2016.03.065

template is subtracted from each channel followed by PCA to remove artifactual components. We applied this approach on the EEG of one subject during 11 Hz tACS and investigated how well heartbeat-related non-linear artifacts were accounted for. We hypothesized that this approach was not able to completely remove the non-linear stimulation artifact, first, because the artifact template subtracted in the first step is temporally not aligned to heartbeat locked modulations, and second, because the variable spatial pattern of non-linear artifacts prevents fully capturing them in few components (Figs. 3 and 4). Indeed, we found that template subtraction did only reduce the main stimulation peak, but did not remove the side-peaks related to non-linear artifacts (Fig. 8a). Furthermore, because heartbeats are randomly positioned relative to stimulation phase, template subtraction destroyed the consistent heartbeat-locked modulation and replaced it with a variable modulation (Fig. 8b). This does not only fail to remove non-linear artifacts, but also complicates tracking them. As hypothesized, the second PCA step did not capture the non-linear artifacts in few components (Fig. 8c). We developed a pipeline based on three different criteria to identify components potentially affected by non-linear stimulation artifacts (Materials and methods). With this, we found about half of the components (36 of 72) as potentially affected. In sum, we concluded that the template subtraction step did not remove non-linear artifacts, but rather complicated tracking them, and that removing few principal components, did reduce, but not entirely remove non-linear artifacts.

Other recent combined MEG and tES studies (Neuling et al., 2015; Soekadar et al., 2013) suggested that adaptive linear spatial filtering (beamforming) (Van Veen et al., 1997) may not only map sensor signals to source space, but also remove stimulation artifacts. To test this for tACS and similar to another recent study (Neuling et al., 2015), we employed beamforming on our MEG recordings during 11 Hz tACS (Fig. 8d–e). At first sight, beamforming results looked promising. Comparing eyes open and eyes closed conditions revealed similar occipital alpha power increases for closed eyes during sham and tACS (Fig. 8d). However, source-level activity during tACS may be confounded by stimulation artifacts, which subtracted out when comparing eyes open and eyes closed conditions. To test this, we exploited our finding that spectra of non-linear artifacts peaked at the stimulation frequency ± heartbeat and respiration frequencies. We hypothesized that, if stimulation artifacts confounded source-level activity, we should observe a spectrally specific correlation between the spatial patterns of source activities at 11 Hz (i.e. the stimulation frequency) and 11 Hz ± heartbeat and respiration frequencies. This is exactly what we found (Fig. 8e). We concluded that beamforming did not remove non-linear stimulation artifacts, but that they were still detectable at the source-level.

In summary, although current artifact-cleaning approaches reduced non-linear artifacts, they did not entirely remove them. Consequently, even after applying these approaches, power enhancements during stimulation may reflect remaining stimulation artifacts rather than neural entrainment.

Discussion

Here, we provide, to the best of our knowledge, the first systematic characterization of transcranial electric stimulation artifacts on EEG and MEG. We uncovered so far unknown non-linear stimulation artifacts, which reflect the modulation of stimulation artifacts by heartbeat and respiration.

Artifact mechanism

Non-linear stimulation artifacts were not caused by modulations of injected currents. Thus, following Ohm's law, we conclude that modulations observed in EEG are due to rhythmic changes of the body's impedance. Indeed, variations of blood volume in vessels caused by heartbeat and respiration, rhythmically modulate body impedance, a phenomenon that is used in impedance plethysmography to monitor cardiodynamic

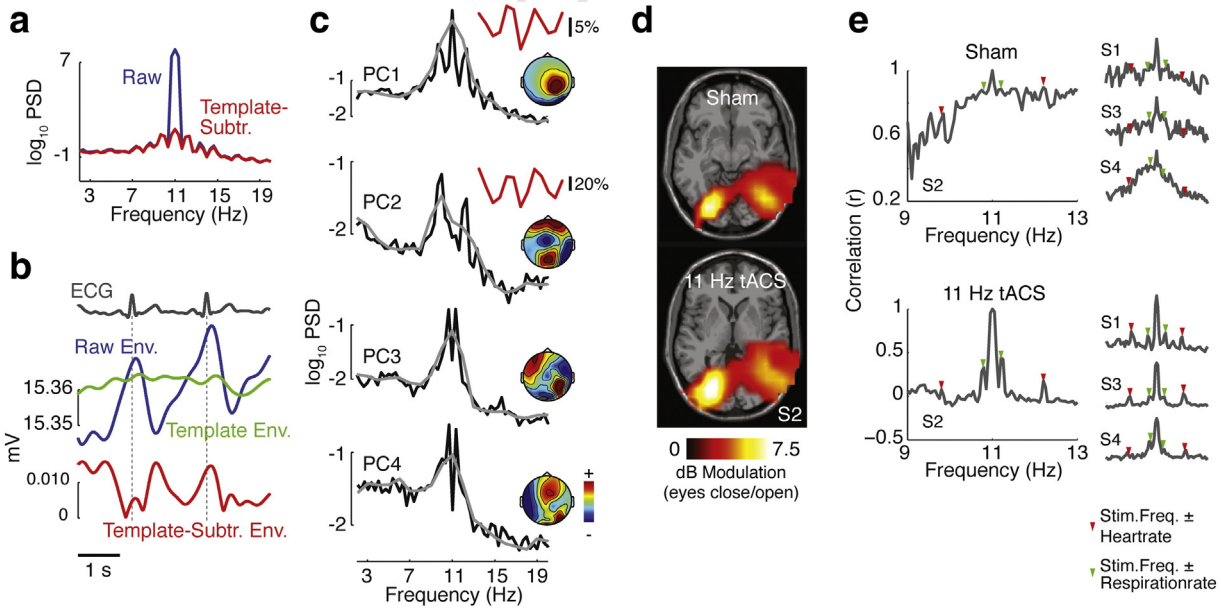

Fig. 8. Evaluation of existing artifact rejection approaches. (*a–c*) Method proposed by Helfrich et al. (2014). (*a*) Power spectral density before and after template subtraction. (*b*) Effect of template subtraction on heartbeat-locked modulations. Envelopes of raw signal, constructed template, and template-subtracted signal during 2 consecutive heartbeats for one EEG channel (O9, 11 Hz tACS). The raw envelope is consistently modulated with the ECG. Template subtraction yields inconsistent modulations reflecting the variable mismatch between raw signal and template (*c*) 4 example PCs. The power spectrum of each PC is shown with high (0.3 Hz, black) and low (1 Hz, gray) resolutions. PC1 has a symmetric power spectrum, an artifactual topography, and its 11 Hz power modulates significantly locked to heartbeats ($P < 0.05$). The small red inset shows %-modulation of 11 Hz power relative to the PC's average power before the R-peak. PC2 is an example PC with heartbeat-locked modulation of 11 Hz power significantly correlated to PC1's heartbeat-locked modulation ($P < 0.05$). PC3 is an example PC with non heartbeat-locked modulations of 11 Hz power significantly correlated to modulations of PC1 ($P < 0.05$). PC4 is an example PC with symmetric spectral peaks around the stimulation frequency. Notably, symmetric spectral peaks are detectable only with high-resolution spectra. (*d, e*) Evaluation of beamforming. (*d*) Source-level contrast between alpha power for eyes closed and eyes open conditions during sham and 11 Hz tACS (masked for $P < 10^{-7}$; subject S2). (*e*) Correlation between the source distribution of 11 Hz power and the power distribution at other frequencies for sham and 11 Hz tACS. Red and green arrows mark the stimulation frequency ± individual average heartbeat and respiration frequencies, respectively.

Please cite this article as: Noury, N., et al., Physiological processes non-linearly affect electrophysiological recordings during transcranial electric stimulation, NeuroImage (2016), http://dx.doi.org/10.1016/j.neuroimage.2016.03.065

parameters (Dornhorst et al., 1952; Kristiansen et al., 2005; Michard, 2005; Nyboer et al., 1950).

For MEG, heartbeat and respiration can modulate the artifact through two different mechanisms. First, changes of body impedance slightly change the distribution of stimulation current on the head, which in turn influences the measured magnetic fields. A second mechanism, that may even contribute more strongly, is the movement of head and body due to respiratory efforts and heartbeats, a phenomenon used in ballistocardiography (Pinheiro et al., 2010). Rhythmic body movements change the distance between stimulation current, both on wires and on the head, and MEG sensors, which in turn leads to rhythmic modulations of the measured magnetic fields.

An important consequence of these mechanisms it that not only heartbeat and respiration, but also other factors that modulate body impedance, such as e.g. sweating or blood pressure, will non-linearly affect stimulation artifacts in EEG. In analogy, also other factors that cause body movement will non-linearly contribute to artifacts in MEG. Beyond the heartbeat and respiration related side-peaks, such slow changes of body impedance and head position may contribute to the width of the artifact peak in the power spectrum (Fig. 2).

Artifact characteristics

The strength of the demonstrated non-linear artifacts renders them highly relevant for the investigation of neural activity. For stimulation currents with 0.5 mA amplitude, which are commonly applied in the field, artifacts for many channels were stronger than the brain signals of interest. In the frequency domain, non-linear artifacts manifest as symmetric contamination of the neighborhood of the stimulation frequency, which corresponds to a spreading of artifacts well up to 10 Hz beyond the stimulation frequency. The extent and strength of this contamination depends on the exact strength and shape of variations in body impedance (EEG) and movements (MEG). Thus, the bandwidth and strength of the non-linear artifact differs between subjects. Furthermore, non-linear artifacts are more easily observed for higher stimulation frequencies where neural activity is weaker.

Importantly, respiration, heart rate, and other physiological parameters such as skin conductance and blood pressure do not only vary between subjects, but also between cognitive states. Thus, when comparing different cognitive states, potential changes in physiological parameters, and thus stimulation artifacts, need to be ruled out or accounted for. For example, a recent tACS study compared lucid and non-lucid dreaming (Voss et al., 2014). Heart and respiration rates change during lucid dreaming (LaBerge et al., 1986). Thus, confounding factors due to such physiological changes should be ruled out when attributing power changes to neural entrainment.

The nature of the non-linear artifact implies that it is independent of the stimulation frequency. This has several important consequences: First, not only the main stimulation frequency, but also all harmonics in the injected current are contaminated by non-linear artifacts. Thus, in particular for low stimulation frequencies like 10 Hz with many nearby harmonics most of the spectrum is contaminated. Second, the spectral bandwidth of non-linear artifacts will be identical for different stimulation frequencies. Thus when comparing different simulation frequencies, potential filtering in the frequency domain should be identical for all frequencies. In contrast, a recent study applied different filters for different stimulation frequencies (Voss et al., 2014). This may be problematic, because different remaining artifacts may in principle induce spurious differences between stimulation frequencies. Third, as our data and other recent results (Marshall et al., 2015) show, non-linear artifacts also affect electrophysiological recordings during tDCS, which is effectively tACS at 0 Hz. Modulations contaminate electrophysiological signals well up to the theta range, while higher frequencies may be clean due to the lack of harmonics (Marshall et al., 2015; Soekadar et al., 2013). It should be noted that artifactual modulations during tDCS have opposite polarities in cathodal and anodal conditions. Thus, their combination with normal E/MCG and, respiration artifacts that are independent of tDCS polarity, may lead to spurious differences of recorded low-frequency power between anodal and cathodal stimulation. This difference between cathodal and anodal stimulation also has to be accounted for in ERP/ERF analyses, when the events of interest interfere with heart and respiration rhythms.

We found that heartbeats and respiration do not only modulate the amplitude of the stimulation artifact, but also its spatial pattern (Figs. 3 and 4). In other words, the stimulation artifact is not projected onto sensors with a constant weight vector, but with a rhythmically varying vector. In turn, this implies that there is no single linear combination of sensor signals that fully captures the artifact. This property is problematic for potential cleaning procedures that are based on linear decompositions or linear filtering such as e.g. PCA, ICA, or beamforming. These methods rely on a constant spatial relationship between sources of interest and sensors. Indeed, our results indicate that removal of few principal components or beamforming does not completely remove non-linear artifacts. Our results accord well with recent findings that beamforming does not eliminate heartbeat-locked tDCS artifacts in MEG (Marshall et al., 2015).

Artifact rejection

Our findings allow for assessing existing artifact rejection approaches and provide critical constraints for developing new model-based rejection methods.

One application of our work is to track and quantify stimulation artifacts through steps of cleaning pipelines to evaluate their performance. We have shown how different characteristics of stimulation artifacts can be used as landmarks to detect stimulation artifacts (Fig. 8). Importantly, the employed approach needs to be adapted to the specific artifact rejection method at hand. For example, as we have shown, certain processing steps may destroy the consistent pattern of heartbeat-locked modulations and therefore a simple heartbeat-locked analysis of envelopes would not be able to track artifacts.

Although the discussed artifact-cleaning methods were not able to fully reject the stimulation artifact, they substantially suppressed it. While this suppression may allow for studying physiological responses (Helfrich et al., 2014; Neuling et al., 2015; Soekadar et al., 2013), spectral changes due to stimulation may still reflect remaining artifacts rather than stimulation induced neuronal entrainment. The same holds for observed changes of spectral modulations by cognitive state (Voss et al., 2014). In this situation, a feasible strategy may be to estimate the strength of residual artifacts as a necessary lower bound for potential entrainment of neural activity. Our work provides the basis for this approach.

Finally, our results pave the way for new artifact-suppressing methods. For example, one may regress out an amplitude-modulation model of the stimulation artifact from the data. This model may be constructed by combining the average kernel of heartbeat and respiration induced modulations with ECG and respiration peaks (Fig. 5). Another option would be to use the output voltage of the stimulation system for cleaning artifacts from EEG, because the output voltage at least partly reflects the underlying changes in body impedance. Similarly, for MEG it may be useful to track head-movements during stimulation and measurements. However, an important caveat for all these approaches is that any error in estimating the artifact amplitude, no matter whether over- or underestimating it, leads to an artifactual increase in signal power at the stimulation frequency, which might be mistaken as neural entrainment.

Apart from artifact suppression methods, also new stimulation approaches may allow for reducing stimulation artifacts. E.g., amplitude-modulated tACS may allow for effectively avoiding stimulation artifacts at the frequency band of interest (Witkowski et al., n.d.). It remains to be determined how the physiological effects of this stimulation approach compare to conventional tACS.

Please cite this article as: Noury, N., et al., Physiological processes non-linearly affect electrophysiological recordings during transcranial electric stimulation, NeuroImage (2016), http://dx.doi.org/10.1016/j.neuroimage.2016.03.065

Conclusion

In sum, we have uncovered and characterized non-linear stimulation artifacts in EEG and MEG during transcranial electric stimulation. These artifacts depend on the subjects' physiological state and are not fully accounted for by current artifact rejection methods. Our work shows how to track these artifacts and paves the way for new artifact rejection approaches.

Funding

Q5 This work was supported by the Centre for Integrative Neuroscience (Deutsche Forschungsgemeinschaft, EXC 307).

Notes

All authors designed the research; N.N. performed the experiments and analyzed the data; N.N. and M.S. wrote the manuscript.

Appendix A. Supplementary data

Supplementary data to this article can be found online at http://dx.doi.org/10.1016/j.neuroimage.2016.03.065.

References

Brittain, J.-S., Probert-Smith, P., Aziz, T.Z., Brown, P., 2013. Tremor suppression by rhythmic transcranial current stimulation. Curr. Biol. 23, 436–440. http://dx.doi.org/10.1016/j.cub.2013.01.068.

Buzsáki, G., Draguhn, A., 2004. Neuronal oscillations in cortical networks. Science 304, 1926–1929. http://dx.doi.org/10.1126/science.1099745.

Dmochowski, J.P., Datta, A., Bikson, M., Su, Y., Parra, L.C., 2011. Optimized multi-electrode stimulation increases focality and intensity at target. J. Neural Eng. 8, 046011. http://dx.doi.org/10.1088/1741-2560/8/4/046011.

Dornhorst, A.C., Howard, P., Leathart, G.L., 1952. Respiratory variations in blood pressure. Circulation 6, 553–558. http://dx.doi.org/10.1161/01.CIR.6.4.553.

Fries, P., 2005. A mechanism for cognitive dynamics: neuronal communication through neuronal coherence. Trends Cogn. Sci. 9, 474–480. http://dx.doi.org/10.1016/j.tics.2005.08.011.

Fröhlich, F., McCormick, D.A., 2010. Endogenous electric fields may guide neocortical network activity. Neuron 67, 129–143. http://dx.doi.org/10.1016/j.neuron.2010.06.005.

Helfrich, R.F., Schneider, T.R., Rach, S., Trautmann-Lengsfeld, S.A., Engel, A.K., Herrmann, C.S., 2014. Entrainment of brain oscillations by transcranial alternating current stimulation. Curr. Biol. 24, 333–339. http://dx.doi.org/10.1016/j.cub.2013.12.041.

Herrmann, C.S., Rach, S., Neuling, T., Strüber, D., 2013. Transcranial alternating current stimulation: a review of the underlying mechanisms and modulation of cognitive processes. Front. Hum. Neurosci. 7, 279. http://dx.doi.org/10.3389/fnhum.2013.00279.

Jensen, O., Mazaheri, A., 2010. Shaping functional architecture by oscillatory alpha activity: gating by inhibition. Front. Hum. Neurosci. 4, 186. http://dx.doi.org/10.3389/fnhum.2010.00186.

Kanai, R., Chaieb, L., Antal, A., Walsh, V., Paulus, W., 2008. Frequency-dependent electrical stimulation of the visual cortex. Curr. Biol. 18, 1839–1843. http://dx.doi.org/10.1016/j.cub.2008.10.027.

Kristiansen, N.K., Fleischer, J., Jensen, M.S., Andersen, K.S., Nygaard, H., 2005. Design and evaluation of a handheld impedance plethysmograph for measuring heart rate variability. Med. Biol. Eng. Comput. 43, 516–521.

LaBerge, S., Levitan, L., Dement, W.C., 1986. Lucid dreaming: physiological correlates of consciousness during REM sleep. J. Mind Behav. 7, 251–258.

Marshall, L., Helgadóttir, H., Mölle, M., Born, J., 2006. Boosting slow oscillations during sleep potentiates memory. Nature 444, 610–613. http://dx.doi.org/10.1038/nature05278.

Marshall, L., Kirov, R., Brade, J., Mölle, M., Born, J., 2011. Transcranial electrical currents to probe EEG brain rhythms and memory consolidation during sleep in humans. PLoS One 6, e16905. http://dx.doi.org/10.1371/journal.pone.0016905.

Marshall, T.R., Esterer, S., Herring, J.D., Bergmann, T.O., Jensen, O., 2015. On the relationship between cortical excitability and visual oscillatory responses—a concurrent tDCS-MEG study. NeuroImage http://dx.doi.org/10.1016/j.neuroimage.2015.09.069.

Michard, F., 2005. Changes in arterial pressure during mechanical ventilation. Anesthesiology 103, 419–428 quiz 449–445.

Neuling, T., Ruhnau, P., Fuscà, M., Demarchi, G., Herrmann, C.S., Weisz, N., 2015. Friends, not foes: magnetoencephalography as a tool to uncover brain dynamics during transcranial alternating current stimulation. NeuroImage 118, 406–413. http://dx.doi.org/10.1016/j.neuroimage.2015.06.026.

Niazy, R.K., Beckmann, C.F., Iannetti, G.D., Brady, J.M., Smith, S.M., 2005. Removal of FMRI environment artifacts from EEG data using optimal basis sets. NeuroImage 28, 720–737. http://dx.doi.org/10.1016/j.neuroimage.2005.06.067.

Nolte, G., 2003. The magnetic lead field theorem in the quasi-static approximation and its use for magnetoencephalography forward calculation in realistic volume conductors. Phys. Med. Biol. 48, 3637. http://dx.doi.org/10.1088/0031-9155/48/22/002.

Nyboer, J., Kreider, M.M., Hannapel, L., 1950. Electrical impedance plethysmography a physical and physiologic approach to peripheral vascular study. Circulation 2, 811–821. http://dx.doi.org/10.1161/01.CIR.2.6.811.

Oostenveld, R., Fries, P., Maris, E., Schoffelen, J.-M., 2011. FieldTrip: open source software for advanced analysis of MEG, EEG, and invasive electrophysiological data. Comput. Intell. Neurosci. 2011, 156869. http://dx.doi.org/10.1155/2011/156869.

Ozen, S., Sirota, A., Belluscio, M.A., Anastassiou, C.A., Stark, E., Koch, C., Buzsáki, G., 2010. Transcranial electric stimulation entrains cortical neuronal populations in rats. J. Neurosci. 30, 11476–11485. http://dx.doi.org/10.1523/JNEUROSCI.5252-09.2010.

Pinheiro, E., Postolache, O., Girão, P., 2010. Theory and developments in an unobtrusive cardiovascular system representation: ballistocardiography. Open Biomed. Eng. J. 4, 201–216. http://dx.doi.org/10.2174/1874120701004010201.

Polanía, R., Nitsche, M.A., Korman, C., Batsikadze, G., Paulus, W., 2012. The importance of timing in segregated theta phase-coupling for cognitive performance. Curr. Biol. 22, 1314–1318. http://dx.doi.org/10.1016/j.cub.2012.05.021.

Romei, V., Gross, J., Thut, G., 2010. On the role of prestimulus alpha rhythms over occipito-parietal areas in visual input regulation: correlation or causation? J. Neurosci. 30, 8692–8697. http://dx.doi.org/10.1523/JNEUROSCI.0160-10.2010.

Romei, V., Driver, J., Schyns, P.G., Thut, G., 2011. Rhythmic TMS over parietal cortex links distinct brain frequencies to global versus local visual processing. Curr. Biol. 21, 334–337. http://dx.doi.org/10.1016/j.cub.2011.01.035.

Schutter, D.J.L.G., Hortensius, R., 2010. Retinal origin of phosphenes to transcranial alternating current stimulation. Clin. Neurophysiol. 121, 1080–1084. http://dx.doi.org/10.1016/j.clinph.2009.10.038.

Schwiedrzik, C.M., 2009. Retina or visual cortex? The site of phosphene induction by transcranial alternating current stimulation. Front. Integr. Neurosci. 3. http://dx.doi.org/10.3389/neuro.07.006.2009.

Siegel, M., Donner, T.H., Engel, A.K., 2012. Spectral fingerprints of large-scale neuronal interactions. Nat. Rev. Neurosci. 13, 121–134. http://dx.doi.org/10.1038/nrn3137.

Singer, W., 1999. Neuronal synchrony: a versatile code for the definition of relations? Neuron 24 (49–65), 111–125.

Soekadar, S.R., Witkowski, M., Cossio, E.G., Birbaumer, N., Robinson, S.E., Cohen, L.G., 2013. In vivo assessment of human brain oscillations during application of transcranial electric currents. Nat. Commun. 4. http://dx.doi.org/10.1038/ncomms3032.

Van Veen, B.D., van Drongelen, W., Yuchtman, M., Suzuki, A., 1997. Localization of brain electrical activity via linearly constrained minimum variance spatial filtering. IEEE Trans. Biomed. Eng. 44, 867–880. http://dx.doi.org/10.1109/10.623056.

Voss, U., Holzmann, R., Hobson, A., Paulus, W., Koppehele-Gossel, J., Klimke, A., Nitsche, M.A., 2014. Induction of self awareness in dreams through frontal low current stimulation of gamma activity. Nat. Neurosci. http://dx.doi.org/10.1038/nn.3719 (advance online publication).

Witkowski, M., Cossio, E.G., Chander, B.S., Braun, C., Birbaumer, N., Robinson, S.E., Soekadar, S.R., n.d. Mapping entrained brain oscillations during transcranial alternating current stimulation (tACS). NeuroImage doi:http://dx.doi.org/10.1016/j.neuroimage.2015.10.024

Womelsdorf, T., Valiante, T.A., Sahin, N.T., Miller, K.J., Tiesinga, P., 2014. Dynamic circuit motifs underlying rhythmic gain control, gating and integration. Nat. Neurosci. 17, 1031–1039. http://dx.doi.org/10.1038/nn.3764.

Zaehle, T., Rach, S., Herrmann, C.S., 2010. Transcranial alternating current stimulation enhances individual alpha activity in human EEG. PLoS One 5, e13766. http://dx.doi.org/10.1371/journal.pone.0013766.

Please cite this article as: Noury, N., et al., Physiological processes non-linearly affect electrophysiological recordings during transcranial electric stimulation, NeuroImage (2016), http://dx.doi.org/10.1016/j.neuroimage.2016.03.065